Pseudobinary Solid-Solution: An Alternative Way for the Bandgap Engineering of Semiconductor Nanowires in the Case of GaP–ZnSe

Wenjin Yang, Baodan Liu, Bing Yang, Jianyu Wang, Takashi Sekiguchi, Staedler Thorsten, and Xin Jiang**

Bandgap engineering of semiconductor nanostructures is of significant importance either for the optical property tailoring or for the integration of functional optoelectronic devices. Here, an efficient way to control the bandgap and emission wavelength is reported for a binary compound semiconductor through alloying with another binary compound. Taking GaP-ZnSe system as an example, the bandgap of quaternary GaP-ZnSe solid-solution nanowires can be selectively tailored in the range of 1.95–2.2 eV by controlling the solubility of ZnSe dopants in GaP host. High-resolution transmission electron microscopy measurement and chemical analyses using an X-ray energy dispersive spectrometer (EDS) demonstrate the solid-solution feature of GaP-ZnSe semiconductor alloy, while X-ray photoelectron spectroscopy (XPS) characterization verifies the formation of some new chemical bonds corresponding to Zn-P and Ga-S bonds in GaP-ZnSe nanowires. The strategy to tailor the optoelectronic property of semiconductor nanostructures through the solid-solution of two different binary compounds represents a general routine to the property modification of all pseudobinary systems and will open more opportunity for their applications in electronics, optics and optoelectronics.

1. Introduction

Bandgap engineering of semiconductors is technologically important for efficient optoelectronic property tailoring and significant device performance improvement and thus plays a key role in semiconductor device integration and application.[1–6] For intrinsic semiconductors, the optical and electrical properties such as conductivity type, carrier density, and mobility, as well as the band structure, are usually confined subjected to their own nature.[4] The electrical conductivity of semiconductors shows a strong impact on the integration of photoelectricity and electrical devices.[7,8] Good examples in this context are field effect transistor and light emitting diode (LED). Consequently, it is crucial to develop efficient methods to modify these properties. This, in turn, will ultimately allow for an enhancement of the performance of any corresponding devices. Previous studies on the tuning of properties of semiconductors have demonstrated that the alloying or solidification of foreign elements (or compound) into the host lattices can lead to significant changes in energy band-gap, electrical transport, lattice constant, and luminescence properties, respectively.[4] Up to date, successful property tuning has been reported for numerous binary and ternary solid-solution systems such as SiGe,[9] ZnCdSe,[10,11] ZnSSe,[2,3] PbSeTe,[12] CdZnTe,[13] InGaN,[1,14] AlGaN,[15] InGaAs,[16] and GaAsP.[17]

The formation of a binary or ternary solid-solution can be regarded as a doping process, in which the dopant element will randomly occupy the position of anions or cations in the host material. For example, a ternary InGaN solid-solution can simply be obtained by substituting Ga with In in GaN. Consequently, this strategy allows for the preparation of InGaN alloys with a defined composition. Compared to binary and ternary semiconductor solid-solutions, quaternary solid-solutions offer an even more powerful path to tailor their optoelectronic properties as anions and cations can be simultaneously substituted

W. Yang, Prof. B. Liu, Dr. B. Yang, Prof. X. Jiang
Shenyang National Laboratory for Materials Science (SYNL)
Institute of Metal Research (IMR)
Chinese Academy of Sciences (CAS)
No. 72, Wenhua Road, Shenhe District, Shenyang 110016, China
E-mail: baodanliu@imr.ac.cn; xjiang@imr.ac.cn
J. Wang, Prof. T. Sekiguchi
Nano-Electronics Materials Unit
National Institute for Materials Science (NIMS)
1-1 Namiki, Tsukuba 305-0044, Japan
Prof. S. Thorsten, Prof. X. Jiang
Institute of Materials Engineering
University of Siegen
Germany, Paul-Bonatz-Str. 9-11, 57076 Siegen, Germany
J. Wang
National Laboratory of Microstructures and
School of Electronic Science and Engineering
Nanjing University
Nanjing 210093, China

DOI: 10.1002/adfm.201404523

Table 1. Possible quaternary $(III\text{-}V)_{1-x}(II\text{-}VI)_x$ solid-solution semiconductor system.

III-V compound	II-VI compound	Solubility (x)	Band gap [eV]	Reference
AlP	ZnS	$x < 0.01$		[35]
AlSb	CdTe	$0 \le x \le 1$	1.4–1.9	[35,36]
AlSb	ZnTe	$x < 0.18$		[35]
GaN	ZnO	$0.05 < x < 0.22$	2.6–2.8	[33,37]
GaP	ZnS	$0 \le x \le 1$	2.2–3.7	[8,19,20,26]
GaP	ZnSe	$0 \le x \le 1$	2.1–2.6	[19,24–26]
GaAs	ZnS	$0 < x < 1$	1.5–3.0	[35,36]
GaAs	ZnSe	$0 \le x \le 1$	1.3–2.6	[19,22]
GaAs	ZnTe	$x \le 0.9$	1.4–2.0	[35,36]
InP	CdS	$0 < x < 1$	1.3–2.6	[35,36]
InP	ZnS	$x < 0.1$, $x > 0.94$		[35]
InP	ZnSe	$x < 0.06$, $x > 0.94$		[35]
InAs	CdTe	$x < 0.33$, $x > 0.7$	0.2–1.5	[35,36]
InAs	HgTe	$0 \le x < 1$		[35]
InSb	CdTe	$x < 0.05$	0.05–0.2	[35,36]

due to the binary nature of the compounds. However, despite all efforts, the defined formation of such materials still remains challenging due to the simple fact that the synthesis of these quaternary solid-solutions involves two individual spontaneous doping processes. Here anions and cations of the dopant replace anions and cations of the host compound during nucleation and crystallization to form a completely new solid phase. Unfortunately, this replacement occurs randomly and often incompletely. The growth conditions of a homogeneous crystallization of such solid-solutions are strictly confined to a local equilibrium.[8] Even slight deviations in composition or temperature will result in a phase separation or might cause the formation of core–shell structures.[18] In fact, almost 50 year ago Yim[19] and co-workers have studied quaternary (III-V)–(II-VI) solid-solutions in different film systems. Their bulky films showed a case-sensitive solubility. In contrast to these films, quaternary solid-solution semiconductors featuring nanoscale dimensions require rather critical growth conditions and well-designed reaction routines to guarantee phase purity.

Even though the formation of solid-solution nanostructures poses a considerable challenge, it is worthwhile to undertake this endeavor as a controlled synthesis of solid-solution nanostructures in different semiconductor system provides alternative routines for the tailoring of optoelectronic properties. Subsequently, achievements in this field will have a strong impact on various electronic nanodevices and functional applications based on these solid-solution nanostructures. Being able to manipulate the formation allows for a potential control over conduction type, carrier density, mobility, resistance, and band-gap of the materials. Most importantly, the growth prerequisite for forming pseudobinary solid-solution proposed within the framework of this study represents a general guideline in order to facilitate the synthesis of different semiconductor groups, which, in turn, paves the way for further fundamental research as well as new technological applications. Recent reports show some progress for nanostructured materials obtained as quaternary solid-solutions from II-VI and III-V semiconductors; e.g., GaPZnS,[20] GaNZnO,[21] GaAsZnSe,[22] and ZnCdSSe.[4] **Table 1** summarizes all known (III-V)–(II-VI) semiconductor alloys in this context.

As key members of the semiconductor family, group III-V and II-VI compounds such as Ga-based nitride and Zn-based oxide as well as sulfide semiconductors have attracted significant research interest due to their peculiar physical and chemical properties making them ideal candidates for numerous technical applications in the field of optics, electronics and photocatalytics.[4,8,20,22–26] In our previous work[8] we have established a general rule for the controlled synthesis of quaternary solid-solutions based on two binary compounds. In this context, the structural homogeneity as well as the chemical compatibility of the initial compounds are the prerequisites for any pseudobinary solid-solution formation and play a key role in achieving a controlled synthesis. Strongly motivated by the potential of the solid-solution approach in the context of tailoring optoelectronic properties we selected zinc-blende-type cubic GaP and ZnSe as initial compounds. This selection was guided by our design rule mentioned above as both materials feature very similar lattice constants. Their difference in band-gap, however, makes them appealing candidates for a band-gap engineering approach based on the tailoring of solubility. In this paper, we demonstrate a successful synthesis of GaP–ZnSe solid-solution nanowires. The process is based on a well-designed two-channel chemical vapor deposition (CVD) method and allows for mass production of these nanowires, which feature lengths on the order of millimeters. The morphology, microstructure, crystallization, and growth process of GaP–ZnSe solid-solution nanowires were systemically studied by scanning electron microscopy (SEM), transmission electron microscopy (TEM), high-resolution transmission electron microscopy (HRTEM) and scanning transmission electron microscopy (STEM). Utilizing spatially resolved energy-dispersive X-ray spectroscopy (EDS), the distribution of composition inside individual

GaP–ZnSe solid-solution nanowires was evaluated. Finally, continuous band-gap engineering in the range of 1.95–2.20 eV was realized by tailoring the solubility of GaP–ZnSe solid-solution nanowires. This achievement unlocks further opportunities for quaternary semiconductor alloy nanowires in various optoelectronic applications.

2. Results and Discussion

2.1. Structural and Chemical Analyses

In order to achieve such GaP–ZnSe solid-solution nanowires featuring an overall solubility, ZnSe and GaP powders of high purity and different stoichiometric ratios were applied as precursors and well-ground graphite with smooth surface was used as substrate for the deposition of materials. The actual growth experiments started out with a pure GaP precursor. In subsequent processes, the ZnSe ratio was gradually increasing until a final experiment was carried out solely utilizing a pure ZnSe precursor. **Figure 1**a shows the correspondent photographs of the complete series of GaP–ZnSe nanowires prepared within the framework of this study. The two samples on the left and right sides correspond to pure ZnSe and GaP nanostructures, respectively; while the remaining nine samples have been synthesized at different nominal composition ratios of GaP:ZnSe. Beginning from the left these ratios are 10:90, 20:80, 30:70, 40:60, 50:50, 60:40, 70:30, 80:20, and 90:10, respectively. At a first glance, all these samples exhibit a yellow appearance without any characteristic variation. In addition to this, SEM observations reveal that all products, with the exception of pure ZnSe with a typical particle-like morphology, feature a wire-like morphology. Figure 1b–d shows typical morphologies of as-synthesized GaP–ZnSe nanowires for nominal composition ratios of ZnSe:GaP=10:90, 30:70, and 70:30, respectively. The processes result in high-density growth of nanowires, which all display smooth surfaces and a wide diameter range of 100–500 nm, respectively (Figure 1e). It can be seen that the average diameter of GaP–ZnSe nanowires exhibits an increasing tendency as the ZnSe ratio increases in initial precursors. For a process time of one hour at a temperature of 1100 °C these GaP–ZnSe nanowires, independent of their composition ratio, feature lengths up to several hundreds of micrometers. Occasionally, some nanowires with a length on the mm-order and a uniform diameter of ≈200 nm can be found. The presence of such ultralong wires implies an extremely fast growth rate exceeding 1 mm h^{-1}. Neither SEM nor TEM images revealed any metal catalysts at the tip-ends of the nanowires investigated. This suggests that the formation of the GaP–ZnSe nanowires is based on a self-reconstruction mechanism of the four constituent elements during the sublimation of the GaP and ZnSe precursors. HRTEM analysis, which was performed on several nanowires, confirmed a superior crystallinity (Figure 1f) of the GaP–ZnSe nanowires. Furthermore, the wires featured a preferential

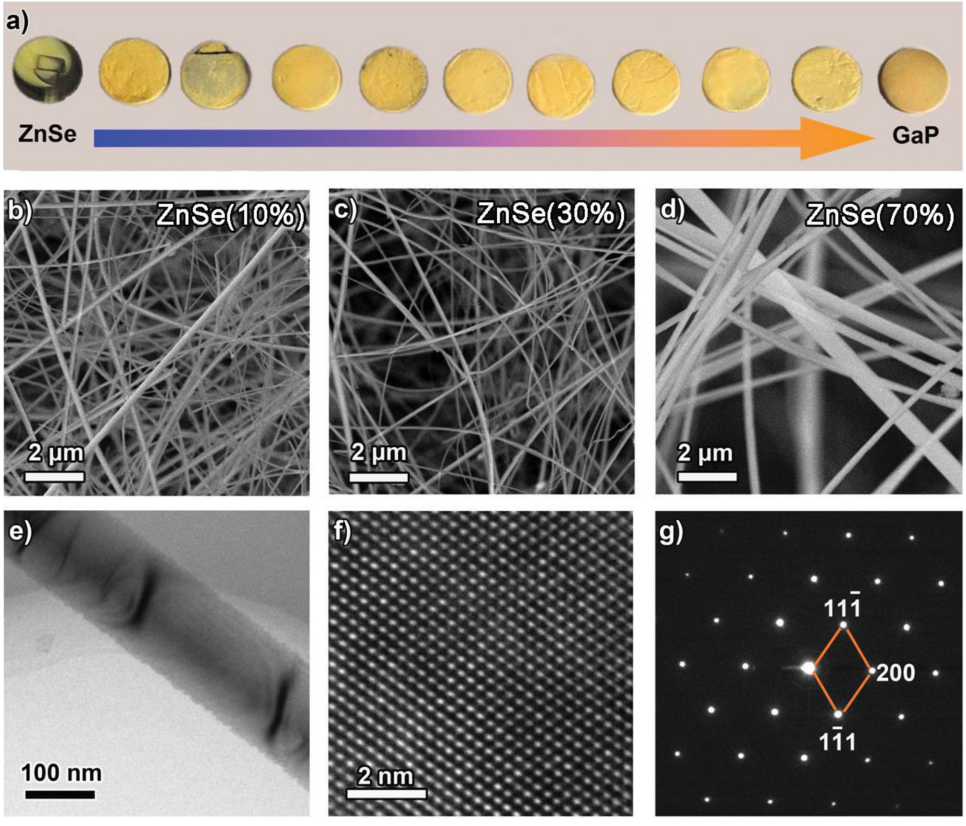

Figure 1. a) Images of GaP–ZnSe solid-solution nanowires featuring different ZnSe nominal composition ratios; b–d) typical morphologies of GaP–ZnSe solid-solution nanowires with different ratios of ZnSe:GaP = 10:90, 30:70, and 70:30, respectively; e) a representative TEM image of a GaP–ZnSe solid-solution nanowire and its corresponding f) HRTEM image and g) SAED pattern.

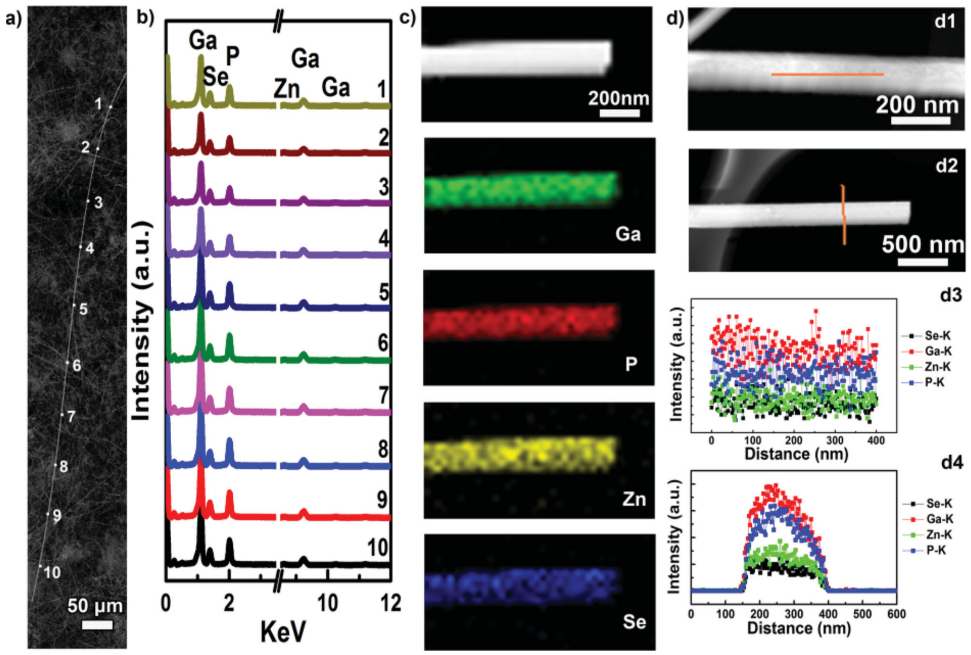

Figure 2. a) Low-magnification SEM image of a long GaP–ZnSe solid-solution nanowire; b) EDS spectra collected from the spots indicated in (a); c) STEM image and its corresponding spatially resolved elemental mapping of Ga, P, Zn, and Se elements in the nanowire; d1,d2) STEM images of GaP–ZnSe solid-solution nanowires and d3,d4) their line-scan composition profiles taken along the radial and axial directions.

orientation along the [110] direction. Both HRTEM images and selected area electron diffraction (SAED) pattern (Figure 1g) verified their single crystal characteristic.

As mentioned above, the formation of quaternary pseudo-binary solid-solution nanowires can be regarded as a random process of simultaneous doping (or substitution) with anions and cations. Compared to binary or ternary solid-solution nanostructures,[3,9,11,27] quaternary solid-solutions are composed of two different binary compounds and consequently consist of four different elements. The increased number of constituting elements undoubtedly complicates the homogeneous solidification process and the realization of phase purity, making the formation of a single-phase solid-solution more challenging. The current study focuses on the GaP–ZnSe system. Here, the four elements, Ga, P, Zn, and Se are able to produce various compounds during nucleation, e.g., binary ZnP, GaP, ZnSe, and GaSe; ternary (GaZn)P, (GaZn)Se, Ga(PSe), and Zn(PSe); and quaternary (GaZn)(PSe). It should be noted that the element of the precursors will often not necessarily take part in the actual reaction and thus binary or ternary solid-solutions might occur in a quaternary system. In particular, any deviation from the standard stoichiometric ratio of a quaternary solid-solution will lead to the appearance of binary or ternary compounds. Additionally, the formation of core–shell structures by phase separation has also been observed and reported for the GaP–ZnS system.[20] Therefore, it is crucial in this study to investigate the constituents of the nanowires along with their spatial distribution. In order to thoroughly examine the composition of the GaP–ZnSe nanowires, EDS was carried out locally as well as in a line-scan and a mapping mode. **Figure 2**a shows a representative GaP–ZnSe nanowire featuring a length of about 1 mm. Figure 2b displays the EDS spectra of ten points along this wire with a spacing ≈80 μm along. All ten spectra show a common curve configuration revealing the presence of four elements (P, Ga, Zn, and Se). As no obvious differences in peak position and intensity can be identified between the ten spots along the ultralong GaP–ZnSe nanowire, it is possible to conclude that the wires feature a uniform composition consisting of Zn, Se, Ga, and P, respectively. Typically, the Ga and P peaks exhibit a higher intensity while the Zn and Se signals appear slightly weaker. This implies that GaP might be regarded as the host component while ZnSe acts as a guest in the GaP–ZnSe solid-solution nanowire. Quantitative analysis on the ten EDS spectra also concluded that P and Ga elements are predominant while Zn and Se are the minor components in GaP–ZnSe solid-solution nanowires and the detailed compositions of the selected nanowires in different regions are listed in Table S1, Supporting Information. The solidification of GaP and ZnSe is also supported by the results of the elemental mapping, shown in Figure 2c. All the four constituent elements show a uniform distribution inside the GaP–ZnSe nanowire. At the same time, their intensity contrast matches well with the peak intensities of the EDS spectra mentioned above. The absence of any sharp composition/phase interface suggests a single phase characteristic of the wire without any phase separation. EDS line-scan analyses along the radial and axial directions provide further compositional information of the GaP–ZnSe nanowire (Figure 2d). Here the radial as well as the axial EDS curves support that GaP and ZnSe are mutually mixed within a GaP-rich nanowire. The solubility (x) of ZnSe in the GaP host lattice is estimated to be in the range of $x = 0.182$–0.209 for a GaP:ZnSe ratio which is close to its optimized value of 4:1. Compared to bulky GaP–ZnSe film system shown in Table 1, the GaP–ZnSe nanowires reveal a narrow solubility range, which may come

from the dimension and size effect in nanoscale. The solubility decrease of quaternary solid-solution nanowires has also been observed in GaP–ZnS system in comparison with its bulky form.[19] It is important to point out that the atomic ratio of each element in the GaP–ZnSe solid-solution nanowire slightly deviates from their initial precursor configuration for the structure stability of the solid-solution. Table S1, Supporting Information lists the actual atomic ratios of P, Ga, Se, Zn in GaP–ZnSe nanowire at nominal ratio of ZnSe:GaP = 70:30 in initial precursor setting. From this table and the chemical analysis using EDS it can be confirmed that the atomic ratio of P and Ga is close to the standard stoichiometric ratio of GaP, whereas the Zn:Se ratio in the wire deviates from the ideal value of 1:1. The resulting solid-solution nanowires are found to contain an increased amount of Se with respect to the Zn present.

The structure and phase purity of the as-synthesized GaP–ZnSe nanowires were further investigated by means of X-ray diffraction (XRD) measurements. All XRD patterns of GaP–ZnSe nanowires featuring different ZnSe composition ratios with the exception of the ZnSe sample exhibit a striking similarity in the range of 20°–60° (Figure S1, Supporting Information). The diffraction peaks in each pattern can be divided into two categories: the peaks centered at 2θ = 26.5°, 42.5°, 44.6°, and 54.5° can be correlated to hexagonal graphite and correspond to (002), (100), (101), and (004) planes, respectively; whereas the remaining peaks can be assigned to a zinc-blend-type cubic structure, which agrees well with the standard XRD data of a pure GaP phase with a lattice constant of a = 0.545 nm (see JCPDS No. 65-2883). For the pure GaP as well as the GaP–ZnSe solid-solution nanowire samples, no impurity-related or unknown peaks were observed. This finding emphasizes the superior phase purity of the as-synthesized nanowires; In contrast to this, the XRD pattern of the ZnSe nanowires revealed some impurity phases, such as hexagonal ZnO. Finally no peak splitting of the (111) peak was observed, which further promotes the conclusion of the single phase state of the GaP–ZnSe solid-solution nanowires prepared in this work. If any mixed GaP or ZnSe phase would exist in the product, the "large" lattice difference between GaP/ZnSe and GaP–ZnSe solid-solution would directly allow for identifying the corresponding peaks within the XRD patterns.

Additional investigations concerning the microstructure and crystallinity of the GaP–ZnSe solid-solution nanowires were conducted by HRTEM. **Figure 3**a–d shows some

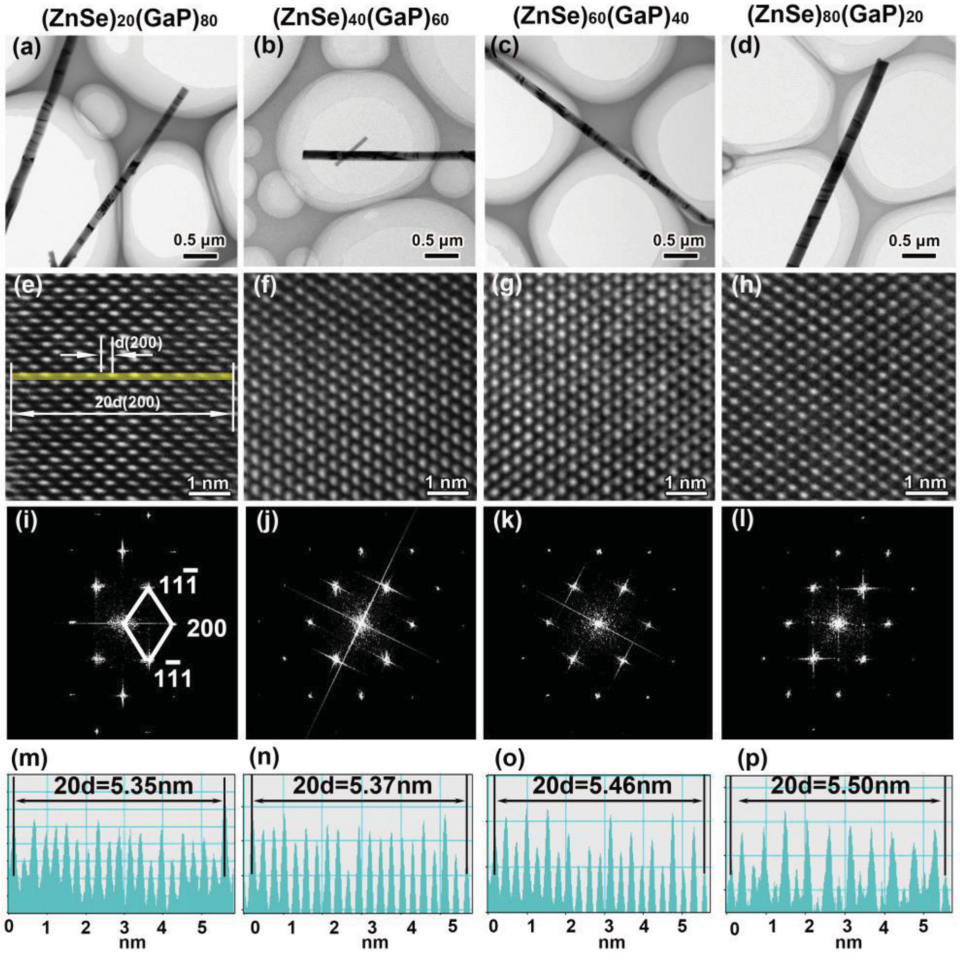

Figure 3. a–d) Low-magnification TEM images of GaP–ZnSe solid-solution nanowires with different ZnSe nominal ratios; e–h) HRTEM images of GaP–ZnSe nanowires shown in (a)–(d); i–l) FFT patterns corresponding to the HRTEM images shown in (e)–(h); m–p) lattice distance measurements of (200) plane based on the HRTEM images shown in (e)–(h).

low-magnification TEM images of GaP–ZnSe solid-solution nanowires with different ZnSe nominal concentrations (ZnSe:GaP = 20:80, 40:60, 60:40, and 80:20, respectively). Clearly, all selected nanowires feature an average diameter of 100–200 nm and no metal catalyst particles were detected at either end of the nanowires. HRTEM analyses performed on nanowires, which were randomly selected, demonstrated that all GaP–ZnSe solid-solution nanowires show good crystallinity displaying a face-centered-cubic structure. Figure 3e–h shows the corresponding HRTEM images of the GaP–ZnSe solid-solution nanowires introduced in Figure 3a–d. It can be noticed that the alloying of GaP and ZnSe still results in a single crystal feature exposing no structural defects such as microtwins or stacking faults. Most importantly, no evidence of any phase separation was found as no crystalline boundaries of any heterostructure were observed during the investigation. Further support for the single crystal as well as solid-solution character of the wires is obtained by studying the fast Fourier transform (FFT) of the HRTEM images given in Figure 3e–h, which show no indication of any overlapping or splitting of the diffraction spots. To precisely calculate the lattice expansion due to solidification, the HRTEM images obtained from experimental observation are first carefully simulated under different sample thickness and defocus values (Figure S2, Supporting Information) and then the planar distances of the (200) lattice plane were measured for all GaP–ZnSe solid-solution nanowires featuring a solubility of $x = 0.182–0.209$. In order to reduce the effect of any potential compositional deviation, the distance of 20 atomic layers in the (200) plane was evaluated using Gatan Digitalmicrograph software, as illustrated in Figure 3e. The corresponding distances are directly shown in Figure 3m–p by measuring the peak spacings. This value gradually increases with an increased amount of ZnSe concentrations in the GaP host lattice. This finding is also confirmed by XRD measurements, in which the (111) peak shows a slight shift towards lower angles with increasing ZnSe concentration in the sample (see Figure S1, Supporting Information). Further calculation on the XRD data also concluded a slight increase of the lattice constant (the (100) planar distance) of GaP–ZnSe solid-solution nanowires as a dependence of ZnSe concentration increase (Table S2, Supporting Information).

The codoping of cation and anion ions in a quaternary solid-solution nanowires system increases the complexity of crystallization and the opportunities for potential inhomogeneities in composition. Compared to the linear change of lattice expansion with respect to ZnSe concentration, which was reported for bulky GaP–ZnSe[19,24] solid-solution films, the lattice variation in our GaP–ZnSe solid-solution nanowires shows a more complex behavior. The reason behind the deviation from a simple linear trend is found in the random nature of the incorporation of Zn and Se atoms into the GaP host lattice. Additionally, the atomic ratio of Zn:Se in the GaP host appears not to be confined to the ideal stoichiometric ratio of 1:1. Compositional analysis of randomly selected GaP–ZnSe solid-solution nanowires utilizing EDS showed a significantly higher concentration of Se compared to Zn. Furthermore, impurities of small clusters that cannot be identified by EDS measurement may also be incorporated locally into the quaternary solid-solution lattice matrix and, in turn, lead to a nonlinear variation of lattice constants, as observed in the GaAs–ZnSe system.[19] On the other hand, the lattice parameters are also closely related to the dimension of the material and will slightly change due to internal stresses and surface tension.[28] When the critical dimension of a material falls into the range of 2–500 nm, significant and complex changes in its lattice parameters will occur. In this context a decrease of crystal size typically leads to an increase in lattice parameters due to internal stresses. Surface tension on the other hand tends to decrease the lattice parameters of nanoscale material. As a result, any nanostructure experiences a combination of both effects on its structure. The arguments presented above give reason to assume that the evolution of lattice parameters in a quaternary solid-solution nanostructure will deviate from the behavior observed in any binary or ternary solid-solution, in which the lattice constants show linearity monotonic expansion or shrinking as a dependence of the dopant concentration. In particular, they show that the nonlinearity of the (200) plane spacing with respect to the ZnSe concentration found in this study seems plausible.[19,26]

2.2. X-Ray Photoelectron Spectroscopy (XPS) Characterization

The chemical compatibility of anodic and cationic elements has been regarded as a key issue in the formation of quaternary solid-solution nanowires. The addition of a binary compound into a binary host compound will undoubtedly alter the local chemical bonds in its lattice and, in turn, render bonding between anodic and cationic ions more complicated due to the difference in chemical valances. As a result, the electronic structure near the conduction and valance bands will be changed.[29] For pure GaP and ZnSe, only Ga–P and Zn–Se bonds exist, respectively, and all cations (Ga and Zn) are surrounded by anions (P and Se). With ZnSe doped into a GaP lattice, the random substitutions of Zn and Se to the Ga and P sites will destroy the initial chemical equilibrium and all the atoms will be forced to reorganize to regain a stable configuration. In this case, the four elements surround each other in some disordered distribution in the solid-solution nanowires. Consequently, this situation will lead to the formation of new chemical bonds such as Ga–Se and Zn–P. In this study we used XPS to study the bonding configurations of GaP, ZnSe and GaP–ZnSe solid-solution nanowires. **Figure 4** shows the XPS spectra of Ga 3d, P 2p, Zn 2p, and Se 3d bonds inside pure GaP, ZnSe, and GaP–ZnSe solid-solution nanowires, respectively. The peak centered at 19.9 eV in Figure 4a corresponds to Ga–P and Ga–Se bonds, whereas the P 2p peak centered at 128.7 eV (Figure 4b, 1) can be divided into two separated bands and implies the existence of Ga–P and Zn–P bonds.[30] Similarly, Zn–Se and Zn–P bonds can be observed with the characteristic Zn 2p peak energies centered at 1024.3 eV (Zn 2p1/2) and 1047.8 eV (Zn 2p3/2), respectively (Figure 4c). Figure 4d shows the characteristic XPS peak of Se 3d with a peak energy centered at 54.2 eV[31] in pure ZnSe and GaP–ZnSe solid solution nanowires. The appearance of the new Ga–Se and Zn–P chemical bonds suggests that Ga element is chemically bonded with neighboring P and Se elements (Figure 4a) whereas P element links to Zn and Ga elements to form Ga–P and Zn–P bonds (Figure 4b, 1) after solid-solution. Compared with pure

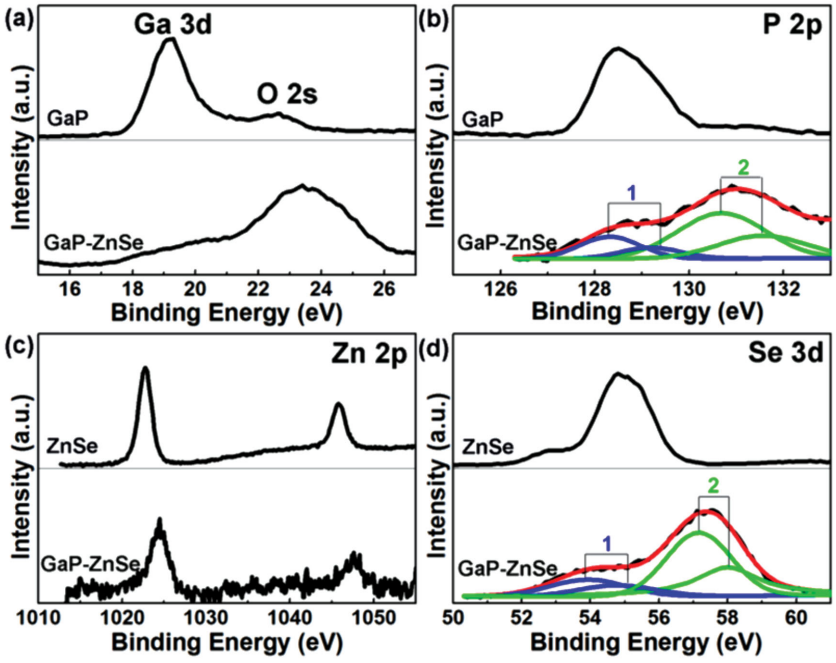

Figure 4. a,b) XPS spectra of Ga 3d and P 2p for GaP and as-prepared GaP–ZnSe solid-solution nanowires; c,d) XPS spectra of Zn 2p and Se 3d for ZnSe and as-prepared GaP–ZnSe solid-solution nanowires.

GaP and ZnSe compounds, the binding energy of Ga–P and Zn–Se bonds is obviously shifted after the alloying of GaP and ZnSe. For example, the binding energies of anions characterized by Ga 3d (Figure 4a) and Zn 2p (Figure 4c) exhibit an increasing tendency after forming solid-solution, whereas the binding energies of cations calibrated with P 2p (Figure 4b, 1) and Se 3d (Figure 4d, 1) moved to the lower energy side. In addition, except for the Ga–P, Ga–Se, Zn–Se, and Zn–P bonds, some P–P (Figure 4b, 2) and P–Se (Figure 4d, 2) bonds centered at 130.9 and 57.3 eV are also observed in GaP–ZnSe solid-solution nanowires.[32] The formation of these P–P and P–Se bonds implies the local enrichment of P atoms in the solid-solution nanowires. It should be mentioned that the solid-solution process of GaP and ZnSe is rather complicated and the substitutions of cations and anions are not strictly complied with the standard stoichiometric ratio for the sake of structural stability in crystallography and the harmony in electronic structure.

2.3. Cathodoluminescence (CL) and Band-Gap Engineering

GaP represents one of the key compound semiconductors and it features an indirect band-gap of 2.27 eV, which corresponds to an intrinsic emission at 550 nm. Due to its promising applications in electrical and optoelectronic devices, it attracted significant research interest. ZnSe on the other hand possesses a direct band gap of 2.7 eV and emits photons at 460 nm. Having both to form a solid-solution obviously holds a number of advantages and represents an attractive option for applications in optoelectronics. First, the incorporation of ZnSe into a GaP host lattice can induce the indirect-to-direct band transition of GaP and thus enhance its photon emission and absorption; Second, the alloying of GaP and ZnSe will also theoretically allow for continuous band-gap engineering in the range of 2.27–2.7 eV. This implies the potential to tailor the emission and absorption wavelength of the GaP–ZnSe nanowires in the visible range of 460–550 nm. Such a visible band recommends these nanowires for an abundance of technologically important applications such as LED, solar-cell, and others. Previous study on the bulk GaP–ZnSe film[19] have demonstrated the possibility of band-gap tailoring through the tuning of solubility. In addition, the electrical transport, photoluminescent wavelength, resistivity and Hall coefficient of GaP–ZnSe solid-solution could also be selectively projected.[24–26] To assess the optical luminescence of GaP–ZnSe nanowires in correlation to their ZnSe concentration, room-temperature CL was used to characterize all the GaP–ZnSe nanowires. **Figure 5**a shows the normalized CL spectra recorded from GaP–ZnSe nanowires that feature initial precursor compositions of $(GaP)_{90}(ZnSe)_{10}$, $(GaP)_{70}(ZnSe)_{30}$, $(GaP)_{50}(ZnSe)_{50}$, $(GaP)_{30}(ZnSe)_{70}$, and $(GaP)_{10}(ZnSe)_{90}$, while their actual (Zn,Se) concentrations are 0.182, 0.185, 0.197, 0.205, and 0.209, respectively. It can be observed that the emission wavelength of these GaP–ZnSe nanowires shifts from 550 to 650 nm as their (Zn,Se) concentration increases from 0.182 to 0.209, thereby covering the red to yellow region in the visible band. It should be noted that the emission bands correspond to the near-band-edge[20] emissions of the GaP–ZnSe nanowires since some energy levels behind the conduction band or above the valance band of GaP will be formed due to the alloying of GaP and ZnSe. Aside from the peak emissions, some shoulders in the range of 600–700 nm can be observed, which can be assigned to some structural point defect or local impurities incorporated in the GaP–ZnSe lattice.[20] Figure 5b shows the band-gap of the GaP–ZnSe nanowires in correlation to their (Zn,Se) concentration. It decreases monotonically from 2.20 to 1.95 eV in the solubility range of ZnSe (x = 0.189–0.209). Surprisingly, all band-gaps (or wavelength) measured in the context of this study exceed the theoretical interval of 2.27–2.7 eV offered by GaP and ZnSe and, additionally, show monotonic decrease. Typically, the introduction of a wide band-gap semiconductor material into a narrow band-gap host will result in a band-gap expansion with respect to the host in binary and ternary solid-solutions.[1] Apparently this is not the case for the quaternary solid-solution studied here. As mentioned above, the formation of a quaternary solid-solution involves simultaneous doping of cations and anions. Consequently, the introduction of these dopants will result in a change of the electronic structures of the valance and conduction band of the host material. Theoretical calculations already predicted a shrinking of the band-gap in the GaP–ZnS system due to a reconstruction of the four elements (S, Zn, P, and Ga). This reconstruction leads to a reduction of the conduction band minimum due to an interaction of

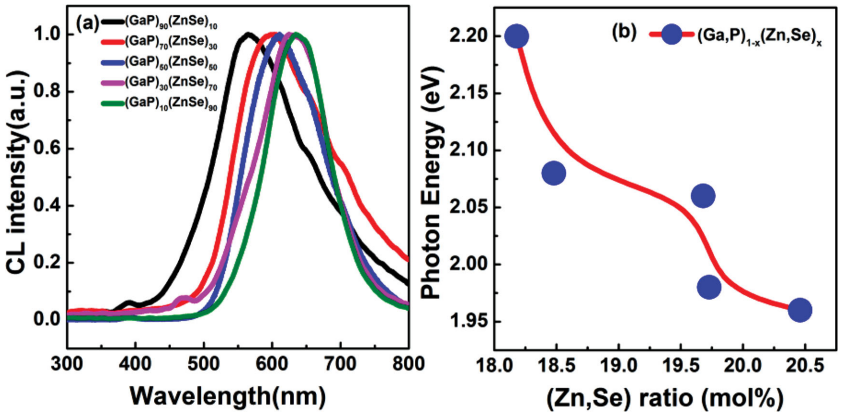

Figure 5. a) Normalized CL spectra of GaP–ZnSe solid-solution nanowires featuring different ZnSe nominal compositions and b) band gap of GaP–ZnSe solid-solution nanowires in correlation to the actual ZnSe ratio.

Ga and S. In this case a minimum band-gap as low as 1.4 eV has been predicted for the GaP–ZnS solid-solution.[29] This prediction is based on the assumption that all Zn atoms are bonded to their nearest P neighbors. A similar shrinking of the band-gap was also observed in the GaN–ZnO solid-solution system. The introduction of ZnO into a GaN lattice host will cause a shift of the absorption edge from the UV to the visible range, making GaN–ZnO solid-solution as an efficient photocatalyst to split water into H_2 and O_2.[33] In contrast to these examples, Pan et al. reported the band-gap engineering in an overall range in ternary and quaternary solid-solution nanostructures.[4–6,22] For example, the band-gap of CdS_{1-x} Se_x ternary solid-solution can be selectively tailored from 1.74 to 2.42 eV through continuous substitution of CdSe with CdS. Correspondingly, the wavelength of CdS_{1-x} Se_x solid-solution nanowires can be tuned in the range of 505–710 nm. Similar band-gap tuning can also be achieved in quaternary ZnCdSSe solid-solution nanowires, in which a broad band-gap modulation in the range of 1.77–3.26 eV can be obtained. In this work, the findings based on the CL emissions of the GaP–ZnSe solid-solution nanowires agrees well with the reports concerning the bulky GaP–ZnSe solid-solution film mentioned above, which show a band-gap narrowing for introducing small amounts of ZnSe into the GaP lattice (ZnSe < 50%). It is also believed that the reorganization of the constituting elements during the formation of the quaternary solid-solution nanowires is responsible for the peculiar band-gap evolution.[4,6,22]

The results presented above all illustrate that the as-synthesized GaP–ZnSe solid-solution nanowires only possess a solubility within a finite range, whereas the bulk GaP–ZnSe solid-solution appears completely miscible.[19] Despite all efforts that have been made it was unfortunately not possible to achieve a wider solubility range as the total percentage of Zn and Se inside the GaP–ZnSe nanowires seems limited to a range between 20% and 30%. We already reported this lower solubility for the GaP–ZnS nanowires in a previous work;[20] other examples for similar findings in the quaternary solid-solution systems of GaP–ZnSe and GaP–ZnS have been described by Tamotsu Uragaki.[26] A sharp increase of formation energy with increasing dopants concentration was observed. This finally led to a decomposition of the solid-solution and an onset of phase separation.[8,20,34] Likewise, a large mismatch in lattice between the host material and the dopant compound can also result in poor solubility.

3. Conclusion

In summary, quaternary GaP–ZnSe solid-solution nanowires with superior crystallinity have been obtained by means of a well-designed CVD method that features two independent reaction channels for precursor transportation. The nanowires show a preferential solubility in the range of $x = 0.182–0.209$. In this context an increase of the ZnSe ratio of the initial precursors led to a corresponding solubility broadening in the GaP host lattice. An introduction of ZnSe into the GaP host resulted also in an expansion of the lattice of the solid-solution nanowires due to the larger lattice constant of ZnSe compared with the one of GaP. The successful alloying of GaP and ZnSe in the solid-solution nanowires was verified by various techniques including HRTEM and EDS. The uniform spatial distribution of each ingredient element inside the nanowire was confirmed by EDS. Room-temperature CL measurements showed that a controlled tailoring of the concentration of ZnSe allowed for a defined continuous optical emissions in the range of 550–650 nm implying a consecutive band-gap engineering from 1.95 to 2.20 eV. However, the solidification of the nanowires studied here displayed an abnormal shrinking of the band-gap with increasing ZnSe content. The successful synthesis of quaternary GaP–ZnSe nanowires with controllable band-gaps reinforces our assertion on the boundary conditions for a controlled formation of pseudobinary solid-solutions and offers further opportunities in optoelectronic nanodevice fabrication.

4. Experimental Section

Synthesis of GaP–ZnSe Nanowire: The GaP–ZnSe quaternary solid-solution nanowires were synthesized by a multichannel CVD route in a conventional horizontal electrical resistance furnace. Typically, a larger quartz tube containing two inner mini-tubes was used as the reactor and was placed into the heating zone of a horizontal three-zone tube furnace. High purity GaP (Aladdin Industrial Corporation, 99.99%) and ZnSe (Alfa Aesar A Johnson Matthey Company, 99.999%) powders mixed with Zn (Sinopharm Chemical Reagent Co., Ltd, AR) and Se powders (Shanghai Xingmei Chemical Co., Ltd, 99.95%) were introduced to the two mini-tubes as the precursors of each constituent element, respectively. In an optimized experiment, the GaP powder was placed at the central temperature zone of the tube furnace whereas the ZnSe powder was placed at the upstream temperature zone, as schematically illustrated in Figure S3, Supporting Information. Graphite substrates featuring diameters of 35 mm were positioned downstream for the deposition of GaP–ZnSe solid-solution nanostructures. Prior to the high temperature reaction, the quartz tube reactor was flushed with high purity Ar gas for 30 min to remove the residual oxygen. Following this step, the three zones of the tube furnace were heated up to 1373, 1373, and 1073 K, respectively, within 110 min, and the reaction was maintained at these temperatures for 1 h at a fixed Ar gas flow rate of 50 sccm until the reaction was finished.

Structural and Compositional Analyses: The morphology of the as-prepared nanowires was characterized by a Zeiss Supra 55 scanning electron microscopy (SEM) operating at 20 KV. The microstructure and composition of the samples were studied and analyzed by using a Tecnai G2 F20 high-resolution field emission transmission electron microscopy in combination with an X-ray EDS. The phase purity of GaP–ZnSe nanowires was identified by means of an X-ray powder diffractometer (XRD, Rigaku RINT 2000) based on Cu Kα radiation. XPS measurements were carried out utilizing an ESCALAB250 spectrometer using Al Kα ($h\nu = 1486.6$ eV) with a spot size of 500 μm.

Optical Property Measurement: The CL spectra of GaP–ZnSe nanowires were measured in an ultrahigh vacuum scanning electron microscopy (UHV–SEM) combined with a Gemini electron gun (Omicron, Germany). For the work presented here, the applied voltage and beam current were set to 5 kV and 1000 pA, respectively.

Supporting Information

Supporting Information is available from the Wiley Online Library or from the author.

Acknowledgements

B. D. Liu would like to thank the Knowledge Innovation Program of Institute of Metal Research (IMR), Chinese Academy of Science (CAS) (Grants No. Y2NCA111A1 and Y3NCA111A1), the Youth Innovation Promotion Association, Chinese Academy of Sciences (Grant No. Y4NC711171)) and Chinese Scholarship Council (Grant No. 201400260067) for the support of this work. S. Thorsten also thanks for the financial support of this work from DAAD with a grant No. 57054770.

Received: December 21, 2014
Revised: February 24, 2015
Published online: March 16, 2015

[1] T. Kuykendall, P. Ulrich, S. Aloni, P. Yang, *Nat. Mater.* **2007**, *6*, 951.
[2] M. Wang, G. T. Fei, Y. G. Zhang, M. G. Kong, L. D. Zhang, *Adv. Mater.* **2007**, *19*, 4491.
[3] H. Xu, Y. Liang, Z. Liu, X. Zhang, S. Hark, *Adv. Mater.* **2008**, *20*, 3294.
[4] A. Pan, R. Liu, M. Sun, C. Z. Ning, *ACS Nano* **2010**, *4*, 671.
[5] J. Xu, X. Zhuang, P. Guo, W. Huang, W. Hu, Q. Zhang, Q. Wan, X. Zhu, Z. Yang, L. Tong, X. Duan, A. Pan, *Sci. Rep.* **2012**, *2*, 820.
[6] a) X. Zhuang, C. Z. Ning, A. Pan, *Adv. Mater.* **2012**, *24*, 13; b) Z. Yang, J. Xu, P. Wang, X. Zhuang, A. Pan, L. Tong, *Nano Lett.* **2011**, *11*, 5085.
[7] L. Li, H. Lu, Z. Yang, L. Tong, Y. Bando, D. Golberg, *Adv. Mater.* **2013**, *25*, 1109.
[8] B. Liu, Y. Bando, L. Liu, J. Zhao, M. Masanori, X. Jiang, D. Golberg, *Nano Lett.* **2013**, *13*, 85.
[9] E. Dailey, P. Madras, J. Drucker, *Appl. Phys. Lett.* **2010**, *97*, 143106.
[10] X. Zhong, M. Han, Z. Dong, T. J. White, W. Knoll, *J. Am. Chem. Soc.* **2003**, *125*, 8589.
[11] H. Lee, P. H. Holloway, H. Yang, L. Hardison, V. D. Kleiman, *J. Chem. Phys.* **2006**, *125*, 164711.
[12] I. U. Arachchige, M. G. Kanatzidis, *Nano Lett.* **2009**, *9*, 1583.
[13] Y. Wang, J. Xu, P. Ren, X. Zhuang, H. Zhou, Q. Zhang, X. Zhu, A. Pan, *Mater. Lett.* **2013**, *105*, 90.
[14] J. Wang, M. Nozaki, Y. Ishikawa, M. S. Hao, Y. Morishima, T. Wang, Y. Naoi, S. Sakai, *J. Cryst. Growth* **1999**, *197*, 48.
[15] K. Forghani, M. Klein, F. Lipski, S. Schwaiger, J. Hertkorn, R. A. R. Leute, F. Scholz, M. Feneberg, B. Neuschl, K. Thonke, O. Klein, U. Kaiser, R. Gutt, T. Passow, *J. Cryst. Growth* **2011**, *315*, 216.
[16] A. V. Thathachary, N. Agrawal, L. Liu, S. Datta, *Nano Lett.* **2014**, *14*, 626.
[17] H. S. Im, C. S. Jung, K. Park, D. M. Jang, Y. R. Lim, J. Park, *J. Phys. Chem. C* **2014**, *118*, 4546.
[18] a) A. Dong, F. Wang, T. L. Daulton, W. E. Buhro, *Nano Lett.* **2007**, *7*, 1308; b) S. A. Ivanov, A. Piryatinski, J. Nanda, S. Tretiak, K. R. Zavadil, W. O. Wallace, D. Werder, V. I. Klimov, *J. Am. Chem. Soc.* **2007**, *129*, 11708.
[19] W. M. Yim, *J. Appl. Phys.* **1969**, *40*, 2617.
[20] B. Liu, Y. Bando, B. Dierre, T. Sekiguchi, D. Golberg, X. Jiang, *ACS Appl. Mater. Interfaces* **2013**, *5*, 9199.
[21] W.-Q. Han, Y. Zhang, C.-Y. Nam, C. T. Black, E. E. Mendez, *Appl. Phys. Lett.* **2010**, *97*, 083108.
[22] Y. Wang, J. Xu, P. Ren, Q. Zhang, X. Zhuang, X. Zhu, Q. Wan, H. Zhou, W. Hu, A. Pan, *Phys. Chem. Chem. Phys.* **2013**, *15*, 2912.
[23] R. S. Wagner, W. C. Ellis, *Appl. Phys. Lett.* **1964**, *4*, 89.
[24] M. Glicksman, *Appl. Phys. Lett.* **1970**, *16*, 366.
[25] P. W. Yu, *J. Appl. Phys.* **1972**, *43*, 4153.
[26] H. Sonomura, T. Uragaki, T. Miyauchi, *Jpn. J. Appl. Phys.* **1973**, *12*, 968.
[27] S. Park, H. Kim, C. Jin, C. Lee, *Curr. Appl. Phys.* **2012**, *12*, 499.
[28] L. Chen, P. Fleming, V. Morris, J. D. Holmes, M. A. Morris, *J. Phys. Chem. C* **2010**, *114*, 12909.
[29] J. N. Hart, N. L. Allan, *Adv. Mater.* **2013**, *25*, 2989.
[30] a) S. S. Kher, R. L. Wells, *Chem. Mater.* **1994**, *6*, 2056; b) V. Samuel, V. J. Rao, *J. Mater. Res.* **1989**, *4*, 185.
[31] a) A. M. Chaparro, C. Maffiotte, M. T. Gutierrez, J. Herrero, *Thin Solid Films* **2000**, *358*, 22; b) T. Izumi, H. Nishiwaki, T. Tambo, C. Tatsuyama, *Appl. Surface Sci.* **1996**, *104*, 570.
[32] J. R. Rollo, G. R. Burns, W. T. Robinson, R. J. H. Clark, H. M. Dawes, M. B. Hursthouse, *Inorg. Chem.* **1990**, *29*, 2889.
[33] K. Maeda, K. Teramura, T. Takata, M. Hara, N. Saito, K. Toda, Y. Inoue, H. Kobayashi, K. Domen, *J. Phys. Chem. B* **2005**, *109*, 20504.
[34] D. A. Bussian, S. A. Crooker, M. Yin, M. Brynda, A. L. Efros, V. I. Klimov, *Nat. Mater.* **2009**, *8*, 35.
[35] U. Rössler, M. Schulz, in *Group IV Elements, IV-IV and III-V Compounds. Part B- Electronic, Transport, Optical and Other Properties* (Eds. O. Madelung, U. Rössler, M. Schulz), Springer, Berlin/Heidelberg **2002**, pp. F-1.
[36] M. Glicksman, W. D. Kraeft, *Solid State Electron.* **1985**, *28*, 151.
[37] M. Yoshida, T. Hirai, K. Maeda, N. Saito, J. Kubota, H. Kobayashi, Y. Inoue, K. Domen, *J. Phys. Chem. C* **2010**, *114*, 15510.